NANO LETTERS

2009
Vol. 9, No. 5
2113-2119

Combining Pattern Instability and Shape-Memory Hysteresis for Phononic Switching

Ji-Hyun Jang,[†] Cheong Yang Koh,[†] Katia Bertoldi,[‡,§] Mary C. Boyce,[*,‡] and Edwin L. Thomas[*,†]

Institute for Soldier Nanotechnologies, Department of Materials Science and Engineering, Massachusetts Institute of Technology, Cambridge, Massachusetts 02139, Institute for Soldier Nanotechnologies, Department of Mechanical Engineering, Massachusetts Institute of Technology, Cambridge, Massachusetts 02139, and Multi Scale Mechanics, TS, CTW, Universiteit Twente, P.O. Box 217, 7500 AE Enschede, The Netherlands

Received February 25, 2009; Revised Manuscript Received April 10, 2009

ABSTRACT

We report a fully reversible and robust shape-memory effect in a two-dimensional nanoscale periodic structure composed of three steps, the elastic instability governing the transformation, the plasticity that locks in the transformed pattern as a result of an increase in glass transition temperature (T_g), and the subsequent elastic recovery due to the vapor-induced decrease in T_g. Solvent swelling of a cross-linked epoxy/air cylinder structure induces an elastic instability that causes a reversible change in the shape of the void regions from circular to oval. The pattern symmetry changes from symmorphic *p6mm* to nonsymmorphic *p2gg* brought via the introduction of new glide symmetry elements and leads to a significant change in the phononic band structure, specifically in the opening of a new narrow-band gap due to anticrossing of bands, quite distinct from gaps originating from typical Bragg scattering. We also demonstrate that numerical simulations correctly capture the three steps of the shape-memory cycle observed experimentally.

Structures with a variety of geometries with nanometer-scale features and submicrometer periodicities have many applications in optics and acoustics,[1−5] and importantly their properties can be quite sensitive to structural details. Reversible control of feature shape in periodic structures via an external triggering stimulus provides an opportunity for tunable devices such as optical/sonic switches. Phononic crystals offer new functionalities including negative effective bulk modulus and effective mass density.[6−8] This is made possible by the purposeful design of the pattern at the requisite length scales to interact with the phonons. Most work to date on phononic structures has concentrated on obtaining large band gaps ($\Delta\omega/\omega_{gap}$) and, to a lesser extent, lensing effects.[9] The former still remains very much an open challenge with no systematically superior way of searching for optimal band structures.[6,10] In addition, dynamic tunability of phononic properties would provide a significant step toward the adoption of phononic crystals for practical device applications such as a switch where the properties change upon the activation of an external stimulus. Ideally, the small triggering field allows the structure to remain in the "linear" regime of operation with the cycling hysteresis to ensure device repeatibility, long device lifetime, etc. In order to induce useful effects within the same frequency window, the pattern change should ideally occur without change in pattern periodicity but at the same time create a significant change in the pattern symmetry/geometry so as to significantly alter the wave propagation behavior and hence phononic properties of the periodic structure.

Recently it was shown that mechanical instability in elastomeric structures can trigger a dramatic pattern transformation[11,12] and can alter the theoretical phononic band gaps.[13] However, the transformed pattern has new periodicit(ies) and reverts to the initial shape upon elimination of the stimulus (solvent swelling or applied mechanical force).[11,12,14−16]

Hence there is a need to find a means to capture the shape changes created by the mechanical instability and then recover the original shape with the same triggering field avoiding dependence on the duration of the triggering field.

* Corresponding authors: Edwin L. Thomas, telephone (617) 253-6901, fax (617) 253-5859, e-mail elt@mit.edu; Mary C. Boyce, telephone (617) 253-2342, fax (617) 258-8752, e-mail mcboyce@mit.edu.

[†] Institute for Soldier Nanotechnologies, Department of Materials Science and Engineering, Massachusetts Institute of Technology.

[‡] Institute for Soldier Nanotechnologies, Department of Mechanical Engineering, Massachusetts Institute of Technology.

[§] Multi Scale Mechanics, TS, CTW, Universiteit Twente.

10.1021/nl9006112 CCC: $40.75
Published on Web 04/24/2009

We utilize a mechanical instability to trigger an abrupt change in the phononic properties. SU8, the material of choice for the fabrication of complex two-dimensional (2D) and three-dimensional structures in microelectromechanical systems, is used as our matrix due to its excellent exposure-contrast as well as good mechanical and thermal stability.[17,18] High rotational symmetries usually promote the ability to obtain a complete band gap by virtue of greater symmetry. This is the case for the band gaps which occur at Brillouin zone boundaries formed via the well-known Bragg type scattering mechanisms. The underlying physical theory that embodies the interpretation and indeed the design of a phononic structure is steeped in the elegance of group theory.[19] Phase transitions typically involve symmetry changes from supergroups to subgroups and afford limited switching capabilities. Another possibility to open a band gap is through inducing anticrossing of bands that possess the same symmetries; their like-symmetries cause them to interact as they cross each other in k-space, leading to level repulsion and, hence, avoided crossing.

The requirements for a complete band gap rest upon several different parameters, including the volume fractions of the two components, the network topology, ratios of the transverse and longitudinal velocities of each component, and the ratios of these velocities between the respective components. The hexagonal void cylinder/epoxy matrix structure requires an air cylinder radius r_c of $>0.44a$ where a is the lattice parameter for existence of a complete band gap;[10] hence our starting *p6mm* structure with $r_c = 0.336a$ ($a = 610$nm, $r_c = 205$ nm) and void volume fraction of 0.41 possesses only partial band gaps. The patterned SU8 film fabricated by interference lithography[20] is 1.5 μm thick with a 700 nm thick SU8 buffer layer adhering the film to a glass substrate.

Figure 1a shows the theoretical band diagram for the *p6mm* structure utilizing a primitive unit cell; note there is only a partial band gap centered at 3.25 GHz ($\Delta\omega/\omega \sim 10\%$) along the $\Gamma-M$ direction. In order to make a comparison to the *p2gg* structure which has two void regions per unit cell, we recalculated the *p6mm* structure utilizing a supercell (Figure 1b). We focus on the change in symmetry of the 20th and 21st bands of the *p6mm* supercell. After the transformation, an avoided crossing occurs in the *p2gg* structure, causing the previous partial band gap to fully open and form a complete gap between the 20th and 21st bands (Figure 1c). The in-plane displacement fields of bands 20 and 21 of the original *p6mm* are shown in Figures 1d and 1e and possess antisymmetric and symmetric displacements about the mirror line, which allows the bands to cross at the K point. Parts f and g of Figure 1 show the displacement fields corresponding to the same two bands in the *p2gg* structure which now possess like symmetries. Their symmetry originates from the glide symmetries present in the *p2gg* structure. A complete discussion is beyond the scope of this Letter and will be addressed in a future work (see Supporting Information for the videos of the displacement fields accompanying mode propagation which show the glide symmetry). The formation of such flat, relatively dispersionless bands (see bands 21 and 22 in Figure 1c) is favored at higher frequencies where the original bands are typically flatter and hence offer the possibility for switchable narrowband filters.

Brillouin light scattering (BLS)[21,22] was employed for experimental verification of the band dispersion relations because of the high frequency (gigahertz) operating range of these phononic crystals. BLS allows for a direct measurement of the phonons present in the structure at a particular scattering vector corresponding to the position in k-space; hence the band diagram is obtained directly in this way. In all of our experiments, the collection was done in the VV geometry; hence only modes which are quasi-longitudinal or mixed modes which have symmetries that can couple to the incident radiation with the set polarization will be detected.[23] In addition, due to the wings of the central Rayleigh peak, frequencies below 1 GHz are not detectable.

The experimentally measured phononic band dispersion superposed onto the theoretical band structure diagrams of the original *p6mm* and the transformed *p2gg* structure are shown in parts a−d of Figure 2. Measurements were taken in the two principal directions (corresponding to [10] and [11]) along the ΓP and ΓQ directions for the original and transformed structure. We plot the experimental data according to the actual scattering angle geometries and superpose onto the theoretical band diagrams that are plotted in the repeated zones scheme, which reflects the actual physical scattering situation more accurately than the reduced zone scheme. There is good agreement between the theoretical band dispersion diagram and the experimentally detected phonon modes. In addition, we also detect two dispersionless modes, which correspond to the glass substrate and the SU8 buffer layer present in our samples. This buffer layer signal also serves as an internal reference for the detected intensity signals. To experimentally illustrate the differences in the phononic band properties of the two structures, parts e and f of Figure 2 compare the frequency spectra taken at the scattering angle $q = 0.00288$ nm^{-1}, in the [10] directions, as indicated. The peaks in the spectra were fitted with a multiple Lorentz oscillator model,[6,23] the insets in parts e and f of Figure 2 providing evidence for the individual (dashed lines) and combined (solid lines) fit to the experimental spectra, showing the clear change in the phononic properties as the structure is transformed from *p6mm* to *p2gg*. It is important to note that, besides a change in the frequencies of modes, the nature of the corresponding displacement fields would be different as well.

We trigger the pattern instability/shape memory effect of the 2D patterned SU-8 utilizing a good solvent to alter the mechanical properties of SU-8 by shifting its T_g through plasticizing the polymer while imparting stress fields through concurrent swelling. This allows the shape transformation to occur as a result of a bifurcation-type elastic instability, which is only accessible in the rubbery regime, as shown in Figure 1h. At relatively small strain fields ($\sim$5%), the SU-8 undergoes a bifurcation elastic instability, inducing the transformation from *p6mm* to a *p2gg* structure.

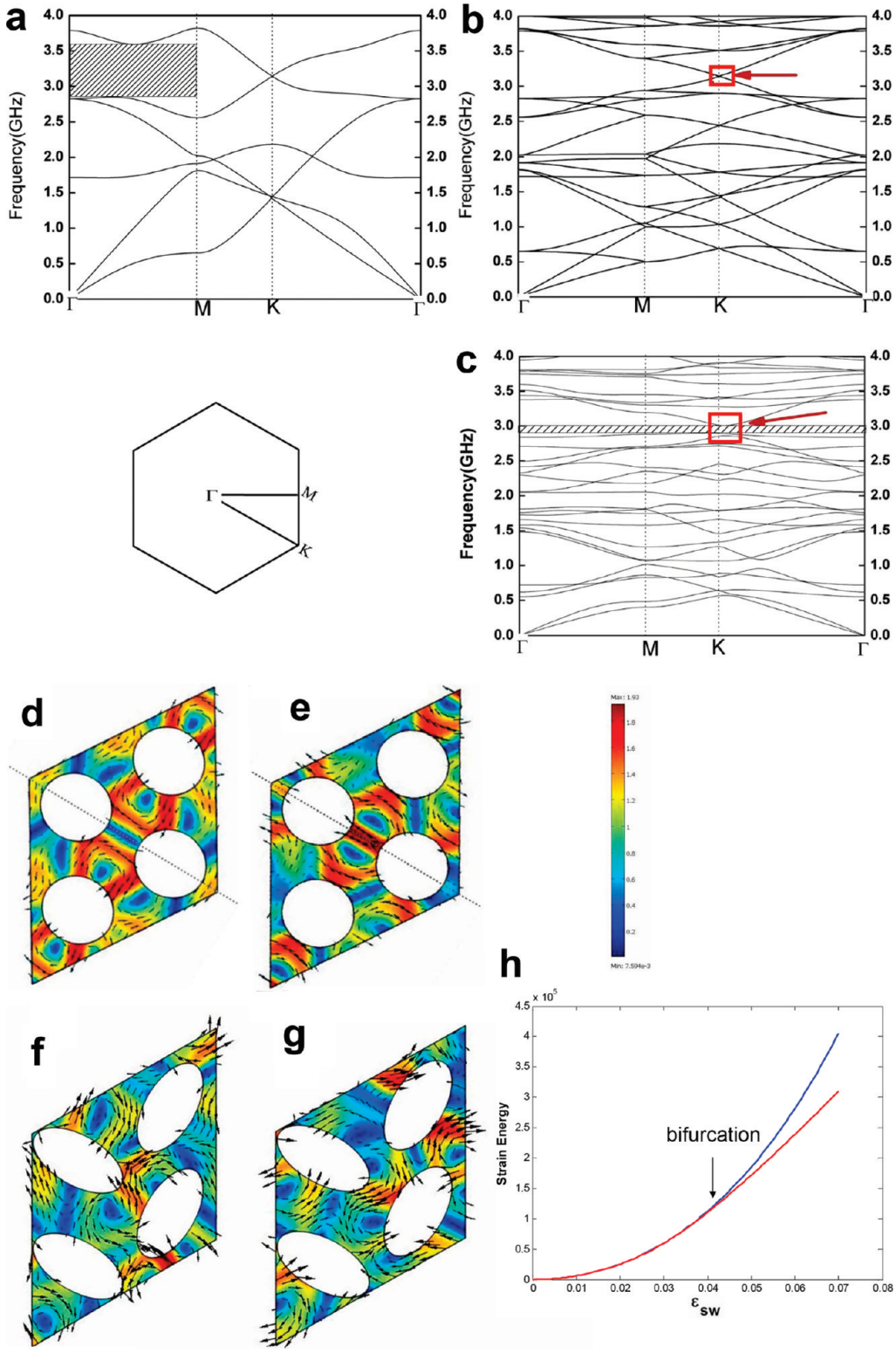

Figure 1. Phononic band structure calculations before and after transformation. Theoretically calculated in-plane phononic band diagrams (a) for the original *p6mm* and (b and c) for the original *p6mm*, using a supercell and the transformed *p2gg* structures. The supercell is utilized in (b) in order to keep the same unit cell size as in (c), for comparison. The red arrow labeled in (b) points to the position in k space where the crossing occurs in the *p6mm*, whereas the arrow in (c) points to that where anticrossing occurs, causing the gap to open. Note also that as a result of the reduced symmetry, several high symmetry points (M, K points) in (c) have the degeneracies lifted in. (d and e) Displacement fields of corresponding modes 20 and 21 in *p6mm* which cross (indicated in Figure 1b). (d) is antisymmetric about the mirror plane while (e) is symmetric, thus crossing is allowed. (f and g) Displacement fields of corresponding modes 20 and 21 in *p2gg* which have interacted to avoid crossing, both (f) and (g) have symmetry corresponding to the glide elements (refer to Supporting Information for attached videos to show clear dependence). All displacement fields have the **k** vector along the [11] direction. (h) The strain energy of the structure as a function of the strain induced by the swelling (ε_{sw}), showing the bifurcation which occurs at a critical swelling strain, favoring transformation from the *p6mm* (blue) to the *p2gg* (red) structures.

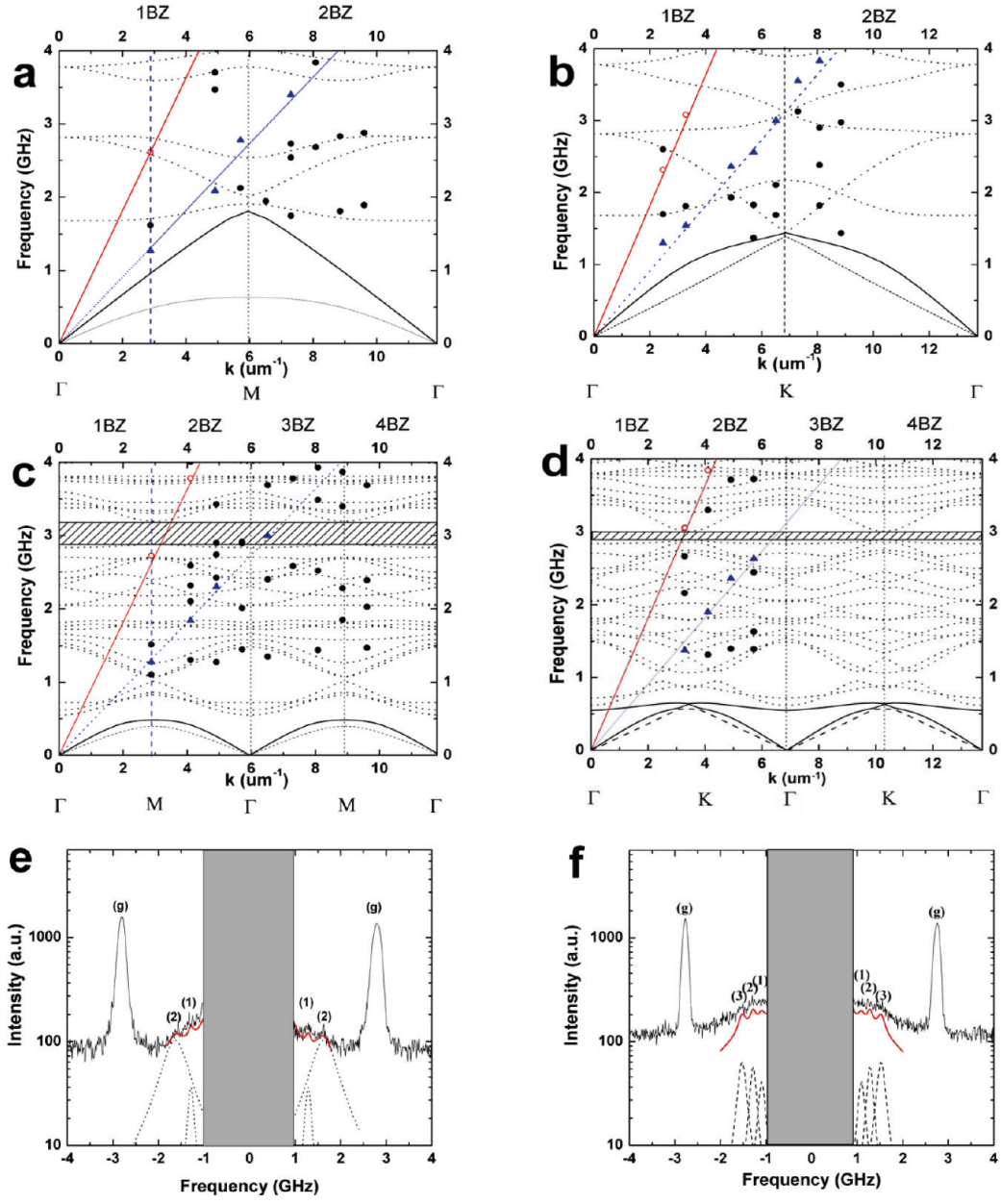

Figure 2. Phononic band structure measurements and calculations. Superposed experimentally measured phononic dispersion modes and the theoretical band dispersion relations in the ΓM and ΓK directions, respectively, for (a and b) the undeformed *p6mm* structure and (c and d) the deformed *p2gg* structure. The solid red line is the theoretical line for the glass; the open red circles are the corresponding experimental points. The dashed blue line is the theoretical line for the SU8 buffer layer present, and the solid blue triangles are the corresponding experimental data points. The solid black lines correspond to the quasi-longitudinal modes, the dashed lines the transverse modes (which cannot be detected), dotted lines correspond to mixed modes of various symmetries corresponding to the respective symmetry group of the structure, with solid circles the respective experimental data points. (e and f) The experimental frequency spectra taken at $q = 0.00287$ nm^{-1} in the ΓM direction of the structures before and after transformation. The frequency spectra correspond to the dashed lines in parts a and c of Figure 2, respectively, which are cuts of the dispersion relation at $q = 0.00287$ nm^{-1}. The solid lines are combined fits to the experimental spectra while the dashed lines are fits for the individual peaks, illustrating the peak positions.

The sequence of proceeding steps for the cyclable shape-memory effect in our 2D patterned SU8 material involves three simple steps (see Figure S1 in Supporting Information).

In step I, the cross-linked network is swollen in a good solvent (NMP (*N*-methylpyrrolindone)) leading to an elastic instability at a certain swelling strain. An ESEM (environmental scanning electron microscope) image of the NMP swollen structure demonstrates the transformation occurring during the swelling process (see Figure S2 in Supporting Information).

In step II the sample is immersed in a large amount of isopropyl alcohol (IPA), a nonsolvent. This causes the outermost surface of the swollen epoxy to lose NMP much faster than the interior. The outer surface regions retract to increase the size of the solvent/nonsolvent filled voids as the epoxy contracts (and the local T_g increases). When this near-surface region attains a T_g above room temperature, it ceases to deform, while the matrix around this "surface skin" continues to contract as the solvent continues to diffuse out. As the IPA/NMP solution is completely evaporated, the

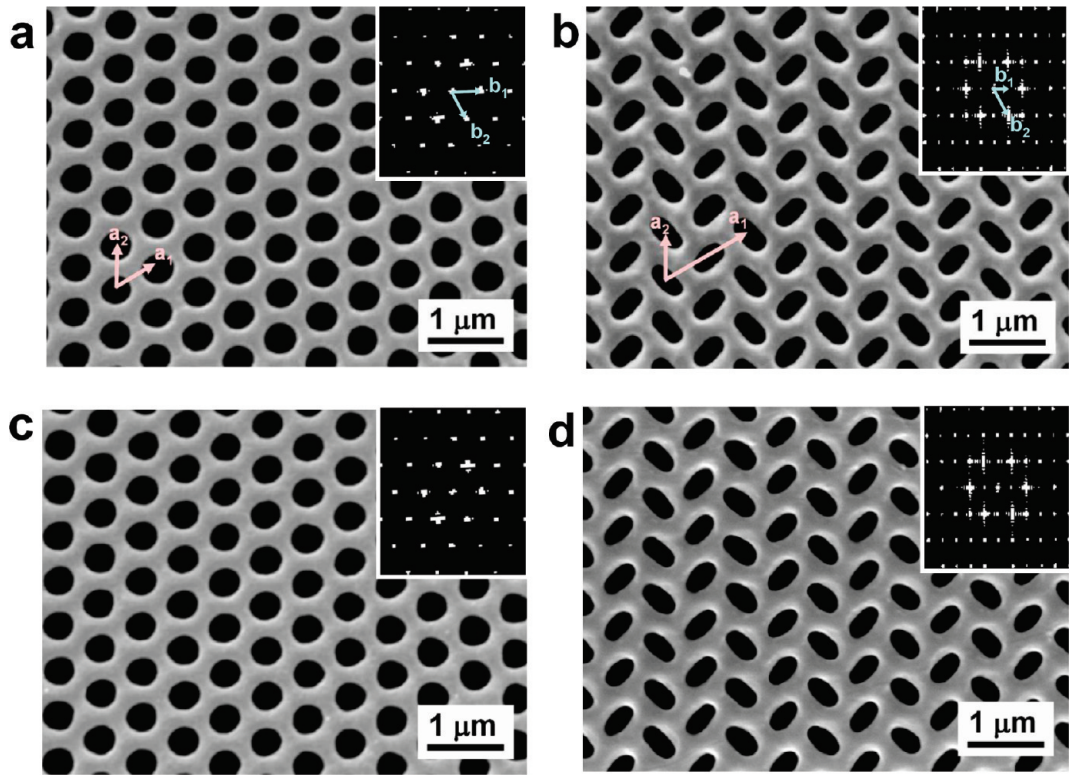

Figure 3. Pattern instability and shape-memory effect for phononic switching. (a) SEM image of original *p6mm* hexagonal lattice with circular air cylinders and a periodicity of 610 nm. (b) SEM image of new (temporary) oval air hole shapes having *p2gg* symmetry due to the liquid solvent swelling induced instability, followed by subsequent nonsolvent freezing of the oval hole shape. (c) SEM image of the structure from (b) after relaxation by solvent vapor treatment. The transformed pattern reverts back to the original structure. (d) SEM image of the temporary air hole shapes in the 10th transformation cycle demonstrating the reversibility of the process. The permanent and temporary shapes (c), (d) in 10th cycle are very similar to the initial shapes (a), (b) at the beginning of the cycle. The insets are calculated FFT power spectra from SEM images, demonstrating that the center to center spacing of the holes is constant during pattern transformation.

sample shrinks in volume but retains the transformed pattern due to the high activation barrier required to modify the rigid epoxy surface regions. Because of the confinement of the patterned SU8 by the highly cross-linked thin (700 nm) SU8 buffer film fixed to the rigid glass substrate, there is no detectable change in the center to center spacing of the voids between deformed and original patterns as indicated in fast Fourier transform (FFT) patterns (Figure 2b).[24]

Step III is the recovery process to the original state (state 1) by a short time (5 min) exposure to NMP vapor. Upon exposure, the deformed sample absorbs a sufficient amount of NMP, to drop the T_g but not enough to retrigger the swelling induced instability, facilitating relaxation of the stresses and reversion to the original sample pattern (Figure 3c).

By reimmersion of recovered samples into NMP, the cycle composed of sequential steps, from the transformation by swelling-induced pattern instability to subsequent freezing to fix the new hole shape, and finally the vapor recovery to release the stress, can be repeated. Key to our process is the hysteresis in the instability arising from the gradient in solvent concentration (creating a gradient in polymer mobility) during the IPA quench step which causes the formation of sufficiently rigid regions that arrest the full recovery to the original structure. Only with subsequent exposure to the solvent vapors is there sufficient simultaneous sample mobility (yet with low swelling so as to avoid the instability regime), to permit the shape change to bring the structure back to its original state with complete solvent evaporation.

To better understand the mechanics of the instability and shape-memory effects[16,25,26] observed, numerical simulations were conducted. The stress−strain behavior of SU-8 is captured using a two-mechanism constitutive model[27] (see Supporting Information). The stress response is decomposed into two mechanisms: the resistance due to stretching and orientation of the molecular network (σ_N) and the resistance arising from intermolecular interactions (σ_V). The shape memory behavior is taken into account by taking σ_v to depend on $(T-T_g)$, where T is room temperature. The intermolecular interactions are negligible when $T > T_g$ and the material is characterized by a rubbery behavior; however, as the T_g moves through room temperature, intermolecular interactions increase and lock in the deformation. The constitutive model is implemented into the commercial finite element code ABAQUS enabling simulation of the swelling, the instability, and the shape memory behaviors. Figure 4c shows the normalized Von Mises stress ($\sigma_{VM}/\sigma_{VM}^{Max}$) and the ratio between the two axes of the holes (b/a) as a function of swelling strain (ε_{sw}) or $T-T_g$ showing clear agreement with the experimentally observed instability and shape-memory behavior. The analysis consists of three steps as indicated in Figure 4a (see Figure S4 in Supporting Information for T_g at each step):

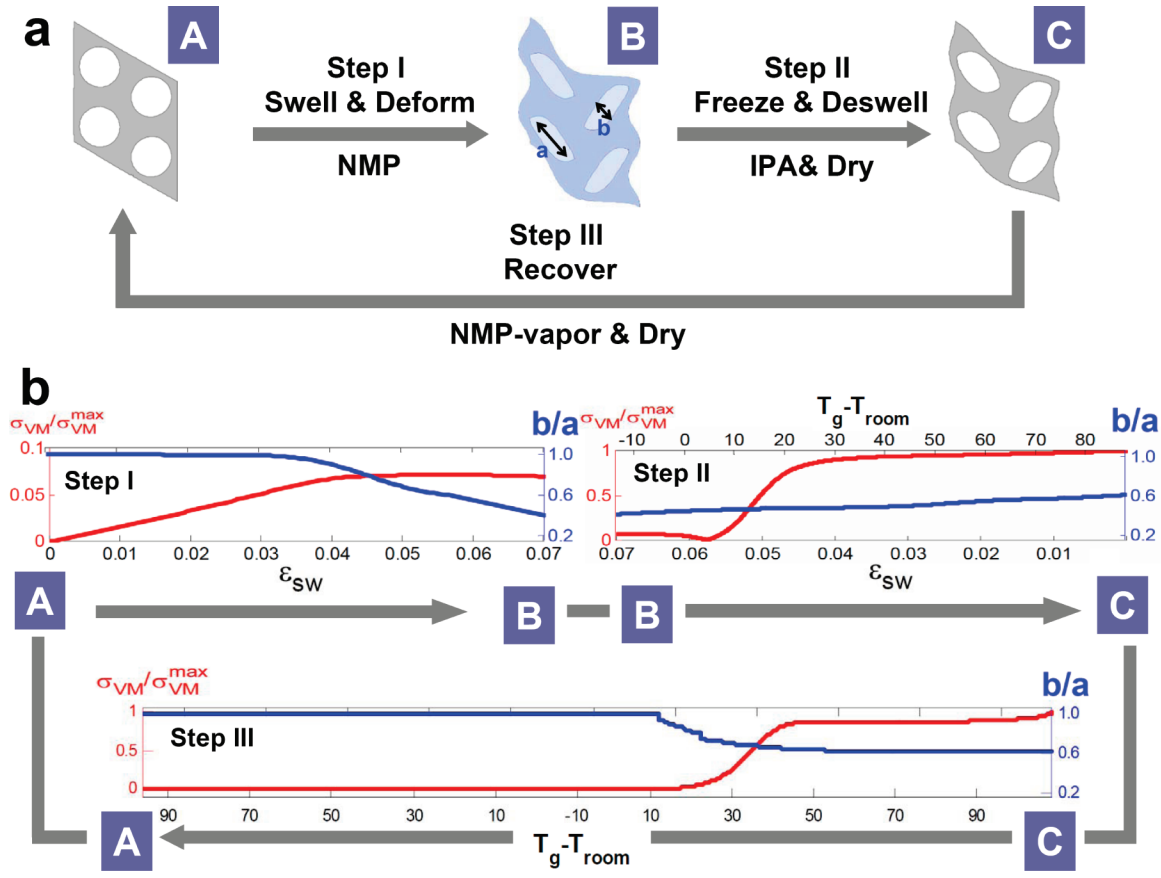

Figure 4. Numerical results for the reversible shape memory cycle. (a) Numerical images of the hexagonal lattice at the beginning of steps I, II, and III. (b) Von Mises stress normalized by its maximum value ($\sigma VM/\sigma VM_{max}$) (red) and voids aspect ratio b/a (blue) vs strain induced by the swelling (ε_{sw}) for steps I and II and vs T_g for step III during the shape-memory cycle.

Step I. Immersion in NMP and swelling. T_g decreases to ~ -10 °C, so that the σ_v vanishes. Bloch wave analysis detects a mechanical instability occurring for a swelling strain $\varepsilon_{sw} = 0.04$ leading to swelling-induced pattern transformation (Figure 4a-B).

Step II. Immersion in IPA and subsequent drying. The material T_g increases to ~112 °C, and the intermolecular interactions increases, making the material much stiffer and providing retention of the transformed pattern (Figure 4a-C).

Step III. NMP vapor treatment and subsequent drying. The material T_g decreases to ~4 °C so that the structure again exhibits a rubbery behavior (σ_v vanishes again) and the initial shape and pattern are elastically recovered (Figure 4a-A).

In conclusion, we have shown a simple way to provide a cyclable shape-memory effect in nanoscale lattices fabricated via IL that allows for potential property control in many useful devices. The internal stress arising due to swelling of cross-linked glassy SU8 structures in a good solvent followed by quenching of the deformed structure in a poor solvent creates a symmorphic to nonsymmorphic structural transformation with the consequence of anticrossing of certain phononic bands resulting in the opening of a complete band gap. Removal of the stress by lowering the T_g via exposure to good solvent vapor returns the structure back to its original state. Numerical simulations correctly capture the shape-memory effect observed experimentally. The pattern instability and shape-memory effects we have shown in the periodic nanoscale structures suggest applications in tunable optical and sonic applications.

Acknowledgment. We thank Steven E. Kooi for technical assistance and Taras Gorishnyy for helpful discussion. This work is supported in part by the Institute for Soldier Nanotechnologies of the U.S. Army Research Office with Contract No. W911NF-07-D-0004 (E.L.T., M.C.B.), the National Science Foundation with Grants CMS-0556211 (E.L.T.) and DMR-0804449 (E.L.T.).

Supporting Information Available: The interference lithographic setup, preparation of samples, basic characterization of the structures with transformed and recovered patterns, details of the constitutive model, numerical simulation of shape-memory effect, numerical calculation of phononic band structure, and BLS measurement. This material is available free of charge via the Internet at http://pubs.acs.org.

References

(1) Parthenopoulos, D. A.; Rentzepis, P. M. *Science* **1989**, *245*, 843.
(2) Qi, M. H.; Lidorikis, E.; Rakich, P. T.; Johnson, S. G.; Joannopoulos, J. D.; Ippen, E. P.; Smith, H. I. *Nature (London)* **2004**, *429*, 538.
(3) Cheng, W.; Wang, J. J.; Jonas, U.; Fytas, G.; Stefanou, N. *Nat. Mater.* **2006**, *5*, 830.
(4) Thomas, E. L.; Gorishnyy, T.; Maldovan, M. *Nat. Mater.* **2006**, *5*, 773.

(5) Jang, J. H.; Ullal, C. K.; Gorishnyy, T.; Tsukruk, V. V.; Thomas, E. L. *Nano Lett.* **2006**, *6*, 740.
(6) Sigalas, M.; Kushwaha, M. S.; Economou, E. N.; Kafesaki, M.; Psarobas, I. E.; Steurer, W. *Z. Kristallogr.* **2005**, *220*, 765.
(7) Ding, Y.; Liu, Z.; Qiu, C.; Shi, J. *Phys. Rev. Lett.* **2007**, *99*, 093904.
(8) Gorishnyy, T.; Maldovan, M.; Ullal, C. K.; Thomas, E. L. *Phys. World* **2005**, *18*, 24.
(9) Lu, M. H.; Zhang, C.; Feng, L.; Zhao, J.; Chen, Y. F.; Mao, Y. W.; Zi, J.; Zhu, Y. Y.; Zhu, S. N.; Ming, N. B. *Nat. Mater.* **2007**, *6*, 744.
(10) Maldovan, M.; Thomas, E. L. *Periodic Materials and Interference Lithography for Photonics, Phononics and Mechanics*; Wiley-VCH: Weinheim, 2008.
(11) Mullin, T.; Deschanel, S.; Bertoldi, K.; Boyce, M. C. *Phys. Rev. Lett.* **2007**, 99.
(12) Zhang, Y.; Matsumoto, E. A.; Peter, A.; Lin, P. C.; Kamien, R. D.; Yang, S. *Nano Lett.* **2008**, *8*, 1192.
(13) Bertoldi, K.; Boyce, M. C. *Phys. Rev. B* **2008**, 77.
(14) Miaudet, P.; Derre, A.; Maugey, M.; Zakri, C.; Piccione, P. M.; Inoubli, R.; Poulin, P. *Science* **2007**, *318*, 1294.
(15) Osada, Y.; Matsuda, A. *Nature (London)* **1995**, *376*, 219.
(16) Liu, C.; Qin, H.; Mather, P. T. *J. Mater. Chem.* **2007**, *17*, 1543.
(17) Jiguet, S.; Bertsch, A.; Judelewicz, M.; Hofmann, H.; Renaud, P. *Microelectron. Eng.* **2006**, *83*, 1966.
(18) Feng, R.; Farris, R. J. *J. Micromech. Microeng.* **2003**, *13*, 80.
(19) Hammermesh, M. 1984, Dover.
(20) Jang, J. H.; Ullal, C. K.; Maldovan, M.; Gorishnyy, T.; Kooi, S.; Koh, C. Y.; Thomas, E. L. *Adv. Funct. Mater.* **2007**, *17*, 3027.
(21) Gorishnyy, T.; Ullal, C. K.; Maldovan, M.; Fytas, G.; Thomas, E. L. *Phys. Rev. Lett.* **2005**, *94*, 115501.
(22) Gorishnyy, T.; Jang, J. H.; Koh, C.; Thomas, E. L. *Appl. Phys. Lett.* **2007**, 91.
(23) Berne, B.; Pecora, R. *Dynamic Light Scattering: With Applications to Chemistry, Biology and Physics*; Dover Publications: Mineola, NY, 2000.
(24) The temporary shape with transformed pattern remains for at least 1 year without any interruption.
(25) Lendlein, A.; Kelch, S. *Angew. Chem., Int. Ed.* **2002**, *41*, 2034.
(26) Qi, H. J.; Nguyen, T. D.; Castro, F.; Yakacki, C.; Shandas, R. *J. Mech. Phys. Solids* **2008**, *56*, 1730.
(27) Wang, L.; Boyce, M. C.; Wen, C.-Y.; Thomas, E. L. *Adv. Funct. Mater.*, **2009**, *19*, published online.

NL9006112